

# Gyroidal mesoporous multifunctional nanocomposites *via* atomic layer deposition†

Cite this: *Nanoscale*, 2014, 6, 8736Jörg G. Werner,<sup>a</sup> Maik R. J. Scherer,<sup>b</sup> Ullrich Steiner<sup>b</sup> and Ulrich Wiesner<sup>\*a</sup>

We demonstrate the preparation of rationally designed, multifunctional, monolithic and periodically ordered mesoporous core-shell nanocomposites with tunable structural characteristics. Three-dimensionally (3D) co-continuous gyroidal mesoporous polymer monoliths are fabricated from a solution-based triblock terpolymer-resol co-assembly and used as the functional templates for the fabrication of free-standing core-shell carbon-titania composites using atomic layer deposition (ALD). The deposition depth into the torturous gyroidal nanonetwork is investigated as a function of ALD conditions and the resulting composites are submitted to different thermal treatments. Results suggest that ALD can homogeneously coat mesoporous templates with well defined pore sizes below 50 nm and thicknesses above 10  $\mu\text{m}$ . Structural tunability like titania shell thickness and pore size control is demonstrated. The ordered nanocomposites exhibit triple functionality; a 3D continuous conductive carbon core that is coated with a crystalline titania shell that in turn is in contact with a 3D continuous mesopore network in a compact monolithic architecture. This materials design is of interest for applications including energy conversion and storage. Gyroidal mesoporous titania monoliths can be obtained through simultaneous titania crystallization and template removal in air.

Received 10th April 2014

Accepted 6th June 2014

DOI: 10.1039/c4nr01948b

www.rsc.org/nanoscale

## Introduction

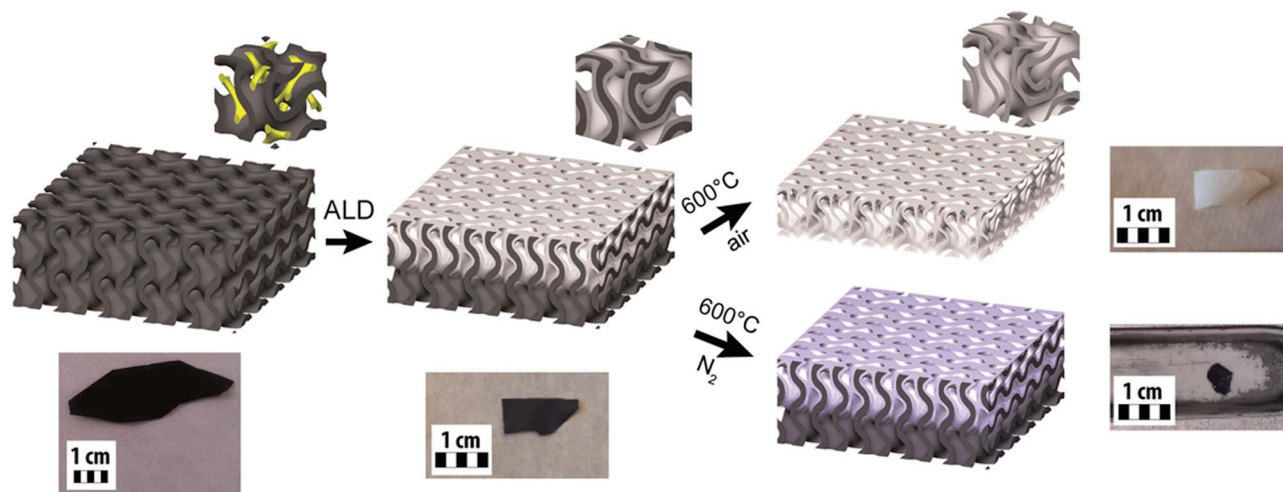
Battery electrode materials suffer from insufficient power densities due to slow solid state diffusion of ions in the active material, poor accessibility of electrolyte to the active material, and low electrical conductivity.<sup>1–3</sup> Nanomaterials, such as nanoparticles, have been successfully applied to increase the rate capability by decreasing the solid state ion diffusion length.<sup>4–6</sup> Additionally, nanocomposites of electrochemically active and electronically conductive materials have been shown to further decrease capacity losses at high-rate operations of electrodes in energy storage systems due to increased conductivity.<sup>7,8</sup> However, in many architectures, the active and conductive materials are still separated on the macroscale or the composite electrodes exhibit large free volumes with low effective electrode densities that yield low volumetric energy densities.<sup>9,10</sup> In this work, we demonstrate the fabrication of rationally designed, free-standing ordered mesoporous core-shell nanocomposites with a double gyroid morphology and tunable structural characteristics. The double gyroid is a cubic, bicontinuous structure that can be described by Schoen's G

surface, a triply periodic minimal surface that divides room into two equally sized volumes without self-intersections.<sup>11</sup> Nature adapts the single gyroid structure in butterfly wings, similarly artificial block copolymers can self-assemble into gyroidal morphologies.<sup>12</sup> The porous three-dimensionally (3D) continuous gyroidal matrix used here represents the gyroidal surface with finite thickness and separates two interpenetrating 3D continuous networks of pores that are enantiomeric to each other. These porous networks consist of triple nodes that are connected by struts (top left of Scheme 1; majority 3D gyroidal matrix in black and two minority 3D continuous pore networks in yellow).<sup>11,13</sup> Flexible gyroidal mesoporous polymeric monoliths with ultralarge pore sizes and large footprint areas were used as functional or sacrificial templates for the fabrication of free-standing micrometer thick core-shell polymer-metal oxide composites or ordered mesoporous titania monoliths, respectively, using atomic layer deposition (ALD) followed by different heat treatments. This deposition technique is widely used in the electronics industry and well studied for flat substrate applications.<sup>14</sup> The self-limiting nature of the deposition process makes ALD an ideal technique for the controlled deposition of conformal thin films with thicknesses of a few nanometers. Despite recent efforts on nanomaterials as substrates for ALD, only a limited amount of work has been performed on purely mesoporous templates.<sup>15–19</sup> Only macroporous (pore sizes > 50 nm) substrates *e.g.* from carbon nanotubes or gold have been demonstrated to result in an ALD penetration depth above 10  $\mu\text{m}$ .<sup>10,20</sup> The use of a

<sup>a</sup>Department of Materials Science and Engineering, Cornell University, Ithaca, NY, USA. E-mail: ubw1@cornell.edu

<sup>b</sup>Cavendish Laboratory, Department of Physics, University of Cambridge, Cambridge, UK

† Electronic supplementary information (ESI) available: Photographs of flexible templates and the Beneq ALD reactor indicating the different sample positioning. See DOI: 10.1039/c4nr01948b



**Scheme 1** Illustration of the process employed for the formation of periodically ordered gyroidal mesoporous multifunctional titania nanocomposites, together with photographs of the resulting materials and gyroidal models illustrating the respective structures. From left to right: monolithic 3D continuous gyroidal mesoporous resin; monolithic 3D continuous gyroidal mesoporous core-shell polymer-titania composite after atomic layer deposition (ALD) of amorphous titania exhibiting decreased deposition thickness away from the top surface; monolithic 3D continuous gyroidal mesoporous crystalline anatase titania (top) and monolithic 3D continuous gyroidal mesoporous core-shell carbon-titania composite (bottom) after heat-treatment at 600 °C in air or inert atmosphere, respectively. The insets show double gyroidal unit cells of the respective structures with indication of the 3D pore (yellow; left) and titania (white; middle and right) connectivity.

functional mesoporous template with pore sizes less than 50 nm and thicknesses above 10  $\mu\text{m}$  as the substrate for another functional material that is deposited using ALD with retention of mesoporosity, to the best of our knowledge, has not been reported to date.

Monolithic mesoporous template films with thickness dimensions of tens of microns, and pore sizes in the nanometer range, are expected to significantly hinder the diffusion of the ALD precursor gases throughout the template. This leads to limitations in the applicability of ALD towards free-standing monolithic mesoporous nanocomposites. In order to quantitatively assess what these limitations are, and thereby the potential of ALD to generate homogeneous multifunctional nanomaterials with applications in energy conversion and storage, we investigated the deposition depth of an ALD oxide coating into a torturous gyroidal porous polymer resin with nanoscopic pore dimensions as a function of the ALD conditions. The ultralarge mesopore size (up to  $\sim 40$  nm) of the template allows for the tunable deposition of more than 10 nm of functional metal oxide coating onto the resin-type substrate while retaining accessibility *via* sufficiently large ( $\sim 20$  nm) and ordered 3D interconnected mesopores. The composites were subsequently converted into ordered multifunctional nanocomposites *via* heat treatment. The resulting materials exhibit a rationally designed nanoarchitecture with a conductive carbon core that is coated with an electrochemically active, crystalline functional material such as titania, which in turn is in contact with a 3D continuous mesopore network. This triple functionality of a conductive core, an active shell and mesoporosity in a compact monolithic architecture of a periodic nanomaterial is expected to be of interest for applications in energy conversion and storage.

## Results and discussion

The fabrication of free-standing core-shell resin-titania composites and their conversion into ordered multifunctional composites is illustrated in Scheme 1. First, free-standing ordered organic-organic hybrid films with gyroidal morphology were fabricated using the structure direction of phenol-formaldehyde resols with the triblock terpolymer poly(isoprene)-*block*-poly(styrene)-*block*-poly(ethylene oxide) (ISO) as described in an earlier study.<sup>21</sup> ISO had a large molar mass of 130 kDa and low polydispersity index of 1.09. For an in-depth structural characterization of the gyroidal monoliths using a combination of small-angle X-ray scattering (SAXS) and transmission and scanning electron microscopy (TEM/SEM), the interested reader is referred to ref. 21. Plasma etching and subsequent pyrolysis of the organic-organic hybrids under inert atmosphere at 450 °C yielded flexible gyroidal mesoporous resin templates with pore sizes of 40 nm, thicknesses of 50–80  $\mu\text{m}$  and a large footprint area of more than 1  $\text{cm}^2$  (Scheme 1 and Fig. S1†). Due to the low pyrolysis temperature and high oxygen content of the precursor, it can safely be assumed that the surface of the polymeric template is covered with oxygen containing functional groups. The monolithic gyroidal mesoporous resins were used as a nanostructured template for the atomic layer deposition (ALD) of titanium dioxide with 250 cycles (unless otherwise noted) at 150 °C using  $\text{TiCl}_4$  and water as precursors. Four different protocols were tested in order to investigate the deposition depth and conformity as a function of the deposition conditions as summarized in Table 1 and described in the experimental section. The thickness of the template was intentionally chosen to be larger than the expected penetration depth for the ALD process for such torturous nanoporous networks in order to investigate the maximum deposition depth

**Table 1** Summary of the ALD conditions employed for the formation of ordered mesoporous multifunctional multicomponent titania nanocomposites

Sample	Cycles	Type	TiCl <sub>4</sub> -pulse time/s	H <sub>2</sub> O-pulse time/s	Soaking time/s
TiO <sub>2</sub> /C-0.4s	250	Flow over	0.4	0.4	—
TiO <sub>2</sub> /C-1s-soak	250	Flow over	1	0.025	6
TiO <sub>2</sub> /C-0.4s-direct	250	Flow through	0.4	0.4	—
TiO <sub>2</sub> /C-1s-direct	250	Flow through	1	1	—
TiO <sub>2</sub> /C-1s-dir-125	125	Flow through	1	1	—

into the template. Two protocols used standard ALD sample positioning in the reactor with the precursor gases pulsed for 0.4 and 1 second, respectively, flowing over the template (see Fig. S1†). Only one of these protocols included a six second soaking time after the precursor gas pulse before the reactor was purged to allow for more efficient diffusion into the template. The resulting samples are referred to as TiO<sub>2</sub>/C-0.4s and TiO<sub>2</sub>/C-1s-soak. For the two other protocols, the templates were directly placed on top of the gas inlet of the reactor in order to direct the flow of precursor gases toward the porous template (see Fig. S1†). Only the influence of pulse time was investigated for this directed flow method. The resulting samples are referred to as TiO<sub>2</sub>/C-0.4s-direct and TiO<sub>2</sub>/C-1s-direct. The ALD template employed here has multiple advantages over commonly used ones: the polymeric resin withstands temperatures well above 100 °C. Such temperatures are typically used for ALD processes, but are inaccessible with normal polymeric templates due to low glass transition temperatures. The template can also be easily burned off in air. In contrast inorganic templates that are commonly used for higher temperature ALD syntheses of nanostructures have to be etched out in tedious post-synthesis steps. A disadvantage over regular polymeric templates is that as a result of cross-linking the template used here cannot be removed by dissolution.

Fig. 1a shows energy-dispersive X-ray spectroscopy (EDX) line-scans of the titanium K-edge from the top surface of freshly cleaved cross-sections of the monolithic carbon–titania nanocomposites. It is noteworthy that the resolution of EDX in a scanning electron microscope (SEM) is on the order of one micrometer. Therefore, the results from this analysis method are only qualitative. It is evident from the data presented in

Fig. 1a, however, that both directed flow of the precursor gases as well as soaking after each precursor pulse significantly increase the deposition depth. The titanium signal for TiO<sub>2</sub>/C-0.4s decreased with increasing distance from the surface and reached less than 15% of the surface signal intensity after 5 μm. The sample with the same pulse time but directed flow of the precursor gases, TiO<sub>2</sub>/C-0.4s-direct, showed a constant titanium signal for the first 4 μm from the top surface, after which it decreased to 15% of the plateau intensity at a depth of 10 μm. Interestingly, the pulse time did not show a distinguishable difference for the directed flow method, as is evident from the overlaying titanium line-scans for TiO<sub>2</sub>/C-0.4s-direct and TiO<sub>2</sub>/C-1s-direct. The line-scan for the sample with soaking time, TiO<sub>2</sub>/C-1s-soak, evidenced the best result. It showed a relatively constant titanium signal for the first 10 μm from the template surface that rapidly decreased to less than 15% of its plateau value at a distance of 14.5 μm from the surface.

The maximum penetration depth of the processes was also investigated using SEM analysis of freshly cleaved edges of the titania composites after heat treatment to remove the polymeric template. The thickness of the remaining titania film after removal of the polymeric membrane can be used to estimate the maximum penetration depth of the ALD process under the respective conditions. The cross-sections of TiO<sub>2</sub>/C-0.4s, TiO<sub>2</sub>/C-1s-direct and TiO<sub>2</sub>/C-1s-soak after polymer removal are shown in Fig. 1b–d, and exhibit a thickness of 4.5, 9 and 12.5 μm, respectively, thereby directly visualizing the increase of ALD depth with increasing pulse and soaking time. These results corroborate that the precursor gas diffusion is significantly hindered by the torturous porosity with nanometer sized pores, but that increased exposure of the nanoporous template to the

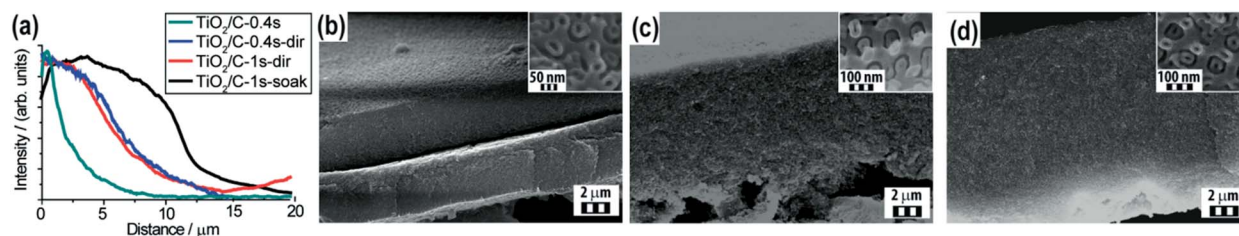


**Fig. 1** (a) Titania EDX line scans from the surface of the as-made polymer–titania composites with 250 deposition cycles. Cross-section SEM images of TiO<sub>2</sub>/C-0.4s (b), TiO<sub>2</sub>/C-1s-direct (c), and TiO<sub>2</sub>/C-1s-soak (d) after removal of the polymeric template by heat treatment. These images directly visualize the increase of ALD depth with increasing pulse and soaking time. Insets depict SEM images of the titania shell structure at higher magnification. Note that in (b) the titania films resulting from both surfaces after removal of the polymer template are collapsed onto each other, whereas in (c) and (d) only one of these films is shown.

reactive gases by either directed flow or soaking of the template in the gas atmosphere can substantially increase the deposition depth.

The deposition conformity and thickness was further investigated using high-resolution SEM on TiO<sub>2</sub>/C-1s-soak, the sample with the highest deposition depth (Fig. 2).<sup>22</sup> For reference, Fig. 2a shows a SEM image of the characteristic (211) gyroidal projection of the porous template before deposition together with a simulation of this projection in the inset. Fig. 2b and c display high-resolution SEM images of the nanocomposite after heat treatment at 600 °C in inert atmosphere at distances of 1 μm and 6.5 μm from the surface, respectively. The layer thickness of the titania “tubes” is approximately 13 nm for both distances from the surface. For comparison the inset of Fig. 2b depicts a simulation of a projection along the [110] zone axis of the gyroid shell, consistent with the images displayed in Fig. 2b–f. Calcination of the polymer–titania composite in air lead to removal of the polymer template and the formation of a free-standing ordered titania monolith (upper right in Scheme 1). The variation of the titania shell thickness can be better evaluated after such template removal. The titania phase, constituting the shell of the two interpenetrating 3D continuous gyroidal pore networks, did not collapse during the calcination. Fig. 2d–f show SEM images of the calcined titania monolith at the top surface, and at distances of 5 μm and 10 μm away from the surface, respectively. While the titania layer thickness appears similar at the top and at 5 μm, it is significantly decreased to approximately 5 nm at a distance of 10 μm from the top (Fig. 2f), as is particularly evident from the insets showing larger magnification images.

Images and data on display in Fig. 2 and 3 reveal the multifunctionality of the materials as illustrated in Scheme 1. Since the polymeric template can either be converted into carbon *via* heat treatment at or above 600 °C in inert atmosphere, or can be burned out at 450 °C in air, two types of multifunctional nanocomposites can be obtained after the ALD process. When heated at 600 °C under nitrogen, the phenolic resin is converted into carbon while the titania shell crystallizes. During this process, mesostructure and mesoporosity are retained as is evident from the images. No change of the shape of the titania phase, collapse of the pores, or disconnection of the titania from the carbon core could be observed by SEM, see Fig. 2b and c. The formation of the carbon core and the crystalline titania shell was corroborated by Raman spectroscopy and X-ray diffraction analysis (XRD), respectively, as shown for the samples using the directed gas flow synthesis conditions with different cycle numbers in Fig. 3 and 4. However, the heat treatment results were similar for all samples, independent of the ALD conditions. Fig. 3a shows XRD data of TiO<sub>2</sub>/C-1s-direct heat treated under different conditions. After pyrolysis at 600 °C in nitrogen (bottom, red trace), the diffraction peaks match the expected reflections for anatase titania (PDF no. 21-1272) with an average crystallite size of 14 nm, approximated using the Scherrer equation for the five main peaks. The crystallite size is on the order of the titania layer thickness, which explains the retention of the periodically ordered core–shell nanostructure. It is important to note that approximation of crystallite size using the Scherrer analysis does not take into account the influence of microstrains on XRD peak broadening. Microstrains are likely in our materials due to titania crystallization

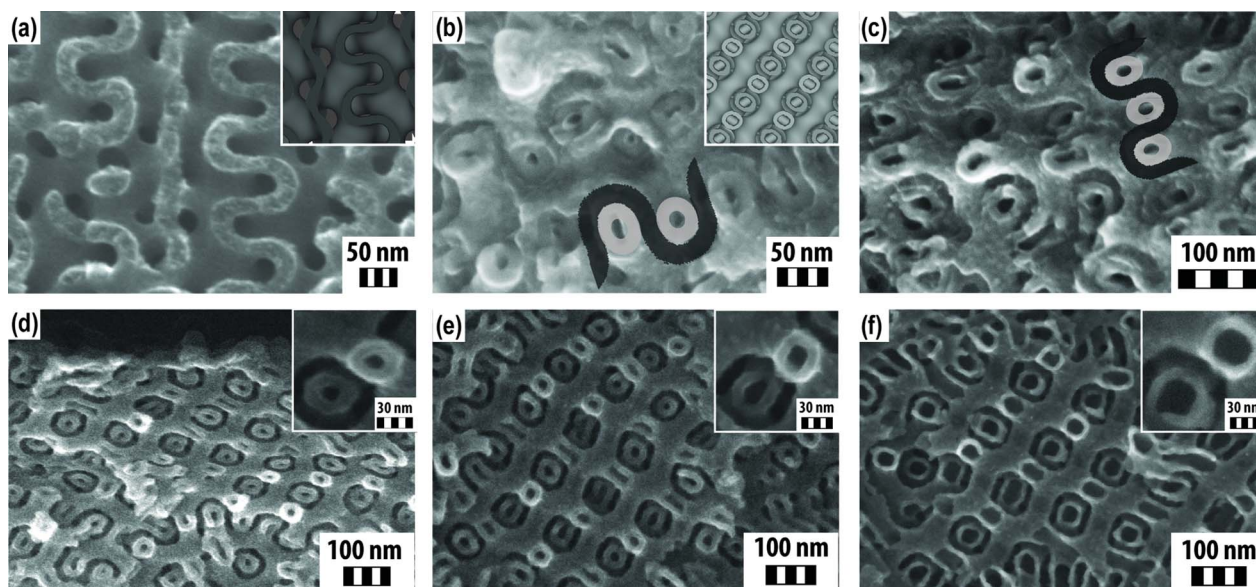


Fig. 2 SEM images of the double gyroidal mesoporous polymer template (a), TiO<sub>2</sub>/C-1s-soak after pyrolysis at 600 °C under nitrogen at distances of 1 μm (b) and 6.5 μm (c) from the surface, and after calcination at 600 °C in air at the surface (d), as well as at 5 μm (e) and 10 μm (f) from the surface, showing a homogeneous titania layer thickness over the first ~7 μm from the template surface. Insets in (a) and (b) show SEM simulations of the double gyroid matrix (211) plane (a) and the double gyroid shell along the [110] zone axis (b). Overlays in (b) and (c) are guides for the eye for a clear identification of the carbon (black) and titania (grey) phases. Insets in (d)–(f) show parts of the respective SEM images at higher magnification facilitating direct titania layer thickness comparison.

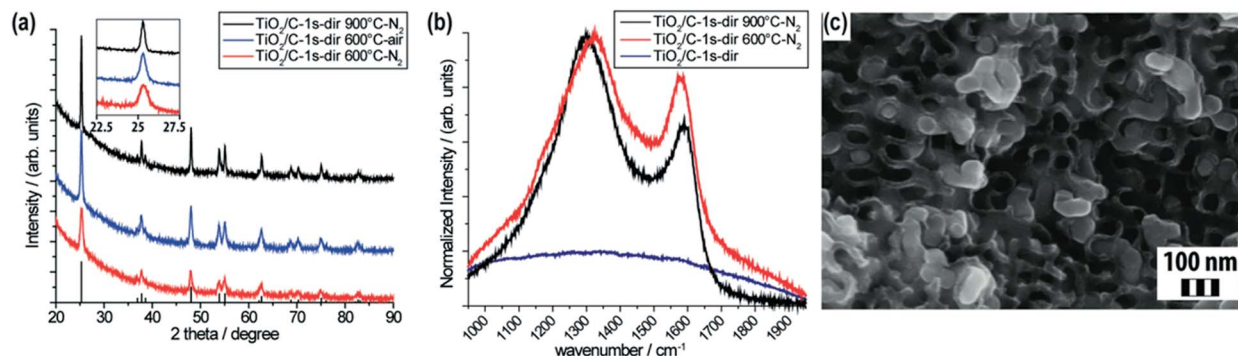


Fig. 3 (a) XRD patterns of TiO<sub>2</sub>/C-1s-direct heat treated under different conditions. (b) Raman spectra of TiO<sub>2</sub>/C-1s-direct before (blue) and after pyrolysis in nitrogen at 600 °C (red) or 900 °C (black) showing the evolution of D- and G-bands, typical for disordered carbon materials. (c) SEM image of TiO<sub>2</sub>/C-1s-direct after pyrolysis in nitrogen at 900 °C revealing the random growth of titania crystallites in the ordered carbon framework.

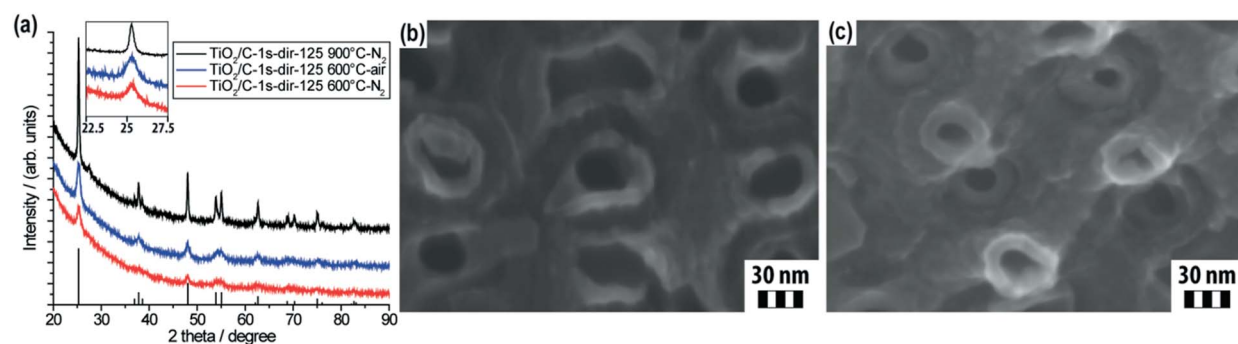


Fig. 4 (a) XRD patterns of TiO<sub>2</sub>/C-1s-direct-125 heat-treated under different conditions. SEM images of TiO<sub>2</sub>/C-1s-direct-125 (b) and TiO<sub>2</sub>/C-1s-direct (c) close to the top surface after pyrolysis at 600 °C in nitrogen showing the titania layer thickness dependence on the ALD cycle number.

on the torturous gyroidal surfaces as well as in confined spaces. When the pyrolysis temperature in nitrogen is raised to 900 °C, the XRD pattern exhibits the same diffraction peaks consistent with anatase titania (top, black trace). Under these higher temperature conditions, however, the crystallite size is increased to 33 nm, which is larger than the titania layer thickness. As revealed in Fig. 3c this further growth of the crystallites resulted in a disruption of the ordered core-shell structure. Large titania crystals are randomly distributed in the carbon matrix. For comparison, after calcination in air at 600 °C leading to polymer resin removal, the crystallite size obtained from the XRD pattern (middle, blue trace) of the resulting monolithic gyroidal mesoporous titania is 17 nm, slightly larger than under inert atmosphere at that temperature.

Raman spectroscopy shows the appearance of D- and G-bands at 1323 or 1296 cm<sup>-1</sup> and 1578 or 1590 cm<sup>-1</sup> after pyrolysis at 600 °C or 900 °C, respectively, with narrowing of the bands with higher temperature (Fig. 3b).<sup>23,24</sup> These bands are indicative for disordered carbon material. The Raman, XRD and SEM data together corroborate the formation of ordered core-shell carbon-titania composites after pyrolysis in nitrogen at 600 °C. However, when heat treated in nitrogen at 900 °C, the growth of the titania crystals disrupts the ordered shell structure while the ordered carbon matrix is retained. There is no

indication of rutile formation in the XRD data. As previously reported, crystalline titania nanomaterials only form the thermodynamically more stable rutile crystal structure above a critical crystallite size, due to the higher surface energy of the rutile phase.<sup>25,26</sup> Interestingly, the crystallite size of over 30 nm observed here for the anatase phase at 900 °C is more than twice as big as previously assumed to be thermodynamically stable from kinetic experiments.<sup>26</sup> We speculate that the rigid carbon support matrix plays a role in the prevention of the anatase-to-rutile phase transformation even at temperatures as high as 900 °C.

The titania deposition thickness on flat substrates can be controlled by the number of ALD cycles. We explored ALD thickness control in our 3D continuous gyroidal nanostructured templates for a depth from the surface of uniform deposition thickness using the directed flow method by reducing the cycle number from 250 to 125. Fig. 4a and b show XRD patterns and a SEM image, respectively, of TiO<sub>2</sub>/C-1s-direct-125 pyrolyzed at 600 °C in nitrogen. From SEM image analysis, the titania deposition thickness is measured to be 9 nm, similar to the Scherrer crystallite size of 10 nm calculated from the XRD pattern. It is noteworthy that in contrast to flat substrates, the layer thickness dependence on cycle number for the deposition inside the torturous gyroidal nanonetwork is not linear (Fig. 4b and c).<sup>14</sup> This may be due both, to increased curvature as well as

decreased accessibility with increasing layer thickness in the mesoporous channels. Tailoring of the titania layer thickness also allows for control of the remaining pore size in the periodically ordered multifunctional core-shell nanocomposites. When pyrolyzed in nitrogen at 900 °C, the crystallite size from the XRD pattern (top, black trace) again increased to 31 nm leading to the disruption of the ordered titania shell structure.

After calcination in air at 600 °C of the as-made TiO<sub>2</sub>/C-1s-direct-125, the template is removed with retention of the ordered titania shell structure, while the oxide crystallizes into the anatase phase. From the XRD pattern in Fig. 4a (middle, blue trace), the crystallite size is calculated to be 10 nm for the ordered mesoporous titania monolith from 125 ALD cycles.

## Conclusions

In this report, we demonstrated the applicability of atomic layer deposition for the formation of multifunctional ordered mesoporous core-shell nanocomposites using self-standing nanoporous templates obtained from block copolymer self-assembly. Functional, free-standing, polymeric templates with gyroidal morphology and ultralarge pore size obtained from a solution-based approach allow for the deposition of more than 10 nm of a functional material such as titania while porosity is retained with large pore sizes above 10 nm. The thickness of the functional shell and remaining pore size can be tailored through the structure of the original template and the number of ALD cycles. Periodically ordered 3D continuous gyroidal mesoporous crystalline titania monoliths were obtained after calcinations of the composite at 600 °C in air. We further demonstrated that the titania shell can also be crystallized at 600 °C under inert atmosphere forming an ordered porous nanocomposite with a conductive 3D continuous gyroidal carbon core and electrochemically active, crystalline shell. Our results demonstrate that purely mesoporous templates in the form of monolithic films with thicknesses up to about 15 μm and 3D co-continuous gyroidal morphology with open and accessible pores on both surfaces can be used for the fabrication of homogeneous multifunctional ordered mesoporous core-shell nanocomposites using standard ALD conditions.

## Experimental section

The structure directing triblock terpolymer poly(isoprene)-*block*-poly(styrene)-*block*-poly(ethylene oxide) (ISO) with a total molecular weight of 129.6 kDa and weight fractions of 15.4%, 31.4% and 53.2% for the three respective blocks was synthesized using sequential anionic polymerization according to published protocols.<sup>21</sup> Phenol-formaldehyde resols with molar mass of less than 500 g mol<sup>-1</sup> were used as the template precursor and synthesized using the well-known basic polymerization of phenol and formaldehyde.<sup>21</sup> Double gyroidal organic-organic hybrids of the triblock terpolymer ISO and phenol-formaldehyde resols were casted as films of approximately 100 μm thickness as described previously.<sup>21</sup> The hybrid films were exposed to argon-oxygen plasma for 30 minutes prior to pyrolysis at 450 °C under nitrogen.

For continuous flow ALD, a Beneq TFS200 system was used with titanium tetrachloride (TiCl<sub>4</sub>, purum, ≥98%, Sigma-Aldrich) and deionized water as the titania precursors. An Arradiance GemStar benchtop ALD system was used for ALD with soaking time. Pulse, purge and soaking times are summarized in Table 1. All depositions were done at 150 °C. The polymer-titania composites were subsequently pyrolyzed at 600 °C or 900 °C under nitrogen, respectively, or calcined at 600 °C in air (see text).

SEM and EDX of composites were carried out on a Zeiss LEO 1550 FE-SEM operating at an accelerating voltage of 10 kV equipped with an in-lens detector and an EDX spectrometer (Quantax EDS, XFlash 3000 silicon drift detector, Bruker Nano GmbH). X-ray diffraction patterns were obtained on an Ultima IV multipurpose X-ray diffraction system from Rigaku using Cu Kα radiation (40 V, 44 mA, wavelength 1.5418 Å) in a 2θ range between 20 and 90° with a speed of 5° min<sup>-1</sup>. For Raman spectroscopy, a Renishaw InVia confocal Raman microscope was used at room temperature in a backscattering geometry, equipped with a 785 nm diode laser as an excitation source focused on the sample with a 50× magnification.

## Acknowledgements

This work was supported as part of the Energy Materials Center at Cornell (emc<sup>2</sup>), an Energy Frontier Research Center funded by the U.S. Department of Energy, Office of Science, Basic Energy Sciences under Award # DE-SC0001086. This work made use of the Cornell Center for Materials Research Shared Facilities which are supported through the NSF MRSEC program (DMR-1120296). The authors also gratefully acknowledge Dr Pedro Cunha for helpful discussions.

## References

- 1 J. M. Tarascon and M. Armand, *Nature*, 2001, **414**, 359–367.
- 2 M. Armand and J.-M. Tarascon, *Nature*, 2008, **451**, 652–657.
- 3 B. Dunn, H. Kamath and J.-M. Tarascon, *Science*, 2011, **334**, 928–935.
- 4 A. S. Arico, P. Bruce, B. Scrosati, J.-M. Tarascon and W. van Schalkwijk, *Nat. Mater.*, 2005, **4**, 366–377.
- 5 P. Poizat, S. Laruelle, S. Grugeon, L. Dupont and J. M. Tarascon, *Nature*, 2000, **407**, 496–499.
- 6 P. G. Bruce, B. Scrosati and J.-M. Tarascon, *Angew. Chem., Int. Ed.*, 2008, **47**, 2930–2946.
- 7 Y.-G. Guo, Y.-S. Hu, W. Sigle and J. Maier, *Adv. Mater.*, 2007, **19**, 2087–2091.
- 8 J. Lee, Y. S. Jung, S. C. Warren, M. Kamperman, S. M. Oh, F. J. DiSalvo and U. Wiesner, *Macromol. Chem. Phys.*, 2011, **212**, 383–390.
- 9 Y. Wang, H. C. Zeng and J. Y. Lee, *Adv. Mater.*, 2006, **18**, 645–649.
- 10 X. Chen, H. Zhu, Y. Chen, Y. Shang, A. Cao, L. Hu and G. W. Rubloff, *ACS Nano*, 2012, **6**, 7948–7955.
- 11 A. H. Schoen, *Infinite periodic minimal surfaces without self-intersections*, NASA Technical Note D-5541, 1970.

- 12 D. A. Hajduk, P. E. Harper, S. M. Gruner, C. C. Honeker, G. Kim, E. L. Thomas and L. J. Fetters, *Macromolecules*, 1994, **27**, 4063–4075.
- 13 D. A. Hajduk, P. E. Harper, S. M. Gruner, C. C. Honeker, G. Kim, E. L. Thomas and L. J. Fetters, *Macromolecules*, 1994, **27**, 4063–4075.
- 14 S. M. George, *Chem. Rev.*, 2010, **110**, 111–131.
- 15 C. Marichy, M. Bechelany and N. Pinna, *Adv. Mater.*, 2012, **24**, 1017–1032.
- 16 E. Kim, Y. Vaynzof, A. Sepe, S. Guldin, M. Scherer, P. Cunha, S. V. Roth and U. Steiner, *Adv. Funct. Mater.*, 2014, **24**, 863–872.
- 17 T. W. Hamann, A. B. F. Martinson, J. W. Elam, M. J. Pellin and J. T. Hupp, *Adv. Mater.*, 2008, **20**, 1560–1564.
- 18 M. A. Cameron, I. P. Gartland, J. A. Smith, S. F. Diaz and S. M. George, *Langmuir*, 2000, **16**, 7435–7444.
- 19 M. Knez, K. Nielsch and L. Niinistö, *Adv. Mater.*, 2007, **19**, 3425–3438.
- 20 M. M. Biener, J. Biener, A. Wichmann, A. Wittstock, T. F. Baumann, M. Bäumer and A. V. Hamza, *Nano Lett.*, 2011, **11**, 3085–3090.
- 21 J. G. Werner, T. N. Hoheisel and U. Wiesner, *ACS Nano*, 2014, **8**, 731–743.
- 22 The titania thickness of the witness sample (flat control substrate) was 12.8 nm.
- 23 F. Tuinstra, *J. Chem. Phys.*, 1970, **53**, 1126.
- 24 T.-H. Ko, W.-S. Kuo and Y.-H. Chang, *Polym. Compos.*, 2000, **21**, 745–750.
- 25 Y. Zhou and K. a. Fichthorn, *J. Phys. Chem. C*, 2012, **116**, 8314–8321.
- 26 H. Zhang and J. F. Banfield, *J. Mater. Chem.*, 1998, **8**, 2073–2076.